THE JOURNAL OF PHYSICAL CHEMISTRY A

Article

pubs.acs.org/JPCA

Indirect Rotational Spectroscopy of HCO^+

Brian M. Siller,[†] James N. Hodges,[†] Adam J. Perry,[†] and Benjamin J. McCall*[,†,‡]

[†]Department of Chemistry and [‡]Departments of Physics and Astronomy, University of Illinois at Urbana−Champaign, Urbana, Illinois 61801, United States

ABSTRACT: Spectroscopy of the ν_1 band of the astrophysically relevant ion HCO^+ is performed with an optical parametric oscillator calibrated with an optical frequency comb. The sub-MHz accuracy of this technique was confirmed by performing a combination differences analysis with the acquired rovibrational data and comparing the results to known ground-state rotational transitions. A similar combination differences analysis was performed from the same data set to calculate the previously unobserved rotational spectrum of the ν_1 vibrationally excited state with precision sufficient for astronomical detection. Initial results of cavity-enhanced sub-Doppler spectroscopy are also presented and hold promise for further improving the accuracy and precision in the near future.

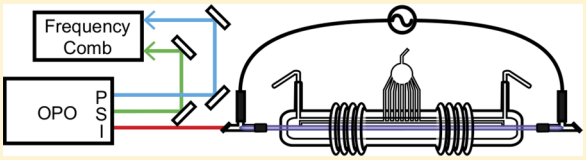

INTRODUCTION

Molecular ions are a particularly challenging group of species to study with optical spectroscopy. Even in laboratory plasmas that are designed to observe only a specific ion, neutral molecules are still orders of magnitude more abundant than their charged counterparts. This is why the most productive techniques for ion spectroscopy tend to have some method for discriminating ionic absorption signals from neutral ones. Since the late 1980s, the predominant tool for this has been velocity modulation spectroscopy (VMS). The groundwork of VMS was laid by Wing et al. in a velocity modulated ion beam,[1] and the first application of VMS as it is known today was by Gudeman et al. in a velocity modulated positive column discharge cell.[2] Since the initial work, the technique has become a mainstay in ion spectroscopy and has been extensively reviewed.[3,4]

Protonated carbon monoxide, HCO^+, was the first ion whose spectrum was acquired using VMS. The R-branch of the ν_1 C−H stretch band was first measured by Gudeman et al. in a positive column discharge cell out to R(18).[2] Shortly after, the P-branch was also observed out to P(10) in a modulated DC glow.[6] After these lines were published, it was another 24 years before any work revisited the ν_1 band, when Verbraak et al. used a continuous wave optical parametric oscillator (cw-OPO) operating in the mid-infrared and a supersonic expansion discharge source to rotationally cool the ions.[7]

The first observation of an HCO^+ rotational transition was via telescope rather than in a laboratory in 1970 by Buhl and Snyder.[8] Because the line that they observed was unidentified at the time, it was referred to as "X-ogen". Later that year, Klemperer suggested that the X-ogen line was due to the $J = 1 \leftarrow 0$ transition of HCO^+.[9] Five years later, Woods et al. confirmed its identity by microwave spectroscopy.[10] Since that time, HCO^+ has been found in a variety of astronomical environments including protoplanetary nebulae,[11] star forming regions,[12] the interstellar medium,[13] and even the comet Hale−Bopp.[14] The abundance of HCO^+ makes it an important participant in the rich chemistry that exists in the interstellar medium. Because of the large rotational constant of HCO^+, its higher rotational transitions exist in the submillimeter/terahertz region. Newer telescopes such as the Atacama Large Millimeter and submillimeter Array (ALMA) and the Stratospheric Observatory For Infrared Astronomy (SOFIA) have submillimeter/terahertz capability. These new astronomical capabilities lend necessity to a relatively simple way to gain laboratory information in that spectral region, a challenging region for laboratory spectroscopy, due in part to the relative scarcity of quality sources and detectors compared to the microwave and infrared spectral regions. In this work, we present a demonstration of how precision rovibrational spectroscopy can be used to infer rotational transitions to precision sufficient to facilitate astronomical searches.

In the case of HCO^+, most of the ground state transitions have been observed up to $J = 17 \leftarrow 16$, with the exception of a few gaps in coverage.[15] Additionally, only a few pure rotational lines have been observed in vibrationally excited states. One such transition is the $J = 3 \leftarrow 2$ rotational transition in the ν_1 first vibrationally excited state.[16] With this single transition combined with our high-precision IR spectrum, the entire rotational spectrum of the ν_1 state can be calculated, limited only by the number of rovibrational lines that have been observed. The technique demonstrated here is also useful for determining high precision rotational constants in excited states.

In this work, we present spectra of the ν_1 fundamental band of HCO^+ acquired using optical heterodyne spectroscopy coupled with VMS (OH-VMS). This technique combines the advantages of the low noise of heterodyne spectroscopy with

Special Issue: Oka Festschrift: Celebrating 45 Years of Astrochemistry

Received: January 17, 2013
Revised: June 11, 2013
Published: June 12, 2013

   dx.doi.org/10.1021/jp400570m | J. Phys. Chem. A 2013, 117, 10034−10040

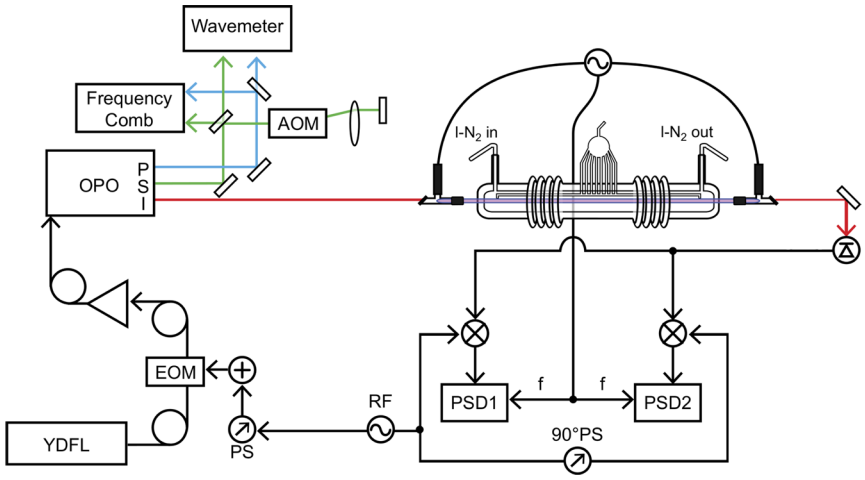

Figure 1. Experimental layout. YDFL, ytterbium-doped fiber laser; EOM, electro-optic modulator; PS, phase shifter; RF, radio frequency generator; OPO, optical parametric oscillator; P,S,I, pump, signal, idler; AOM, acousto-optic modulator; PSD, phase-sensitive detector.

the ion-neutral discrimination of VMS. Our instrument utilizes a cw-OPO tunable from 3.2 to 3.9 μm, and produces ions within a liquid nitrogen cooled positive column discharge cell. Optical frequency comb calibrated scans were acquired and fit with sub-MHz precision, and the resulting fits were used to calculate rotational transitions for the ground state and the first vibrationally excited C−H stretch state. These calculations result in the first experimental observation, albeit indirectly, of the $J = 3 \leftarrow 2$ transition in the ground state and the complete determination of the rotational spectrum up to $J = 10 \leftarrow 9$ in the ν_1 first excited state.

EXPERIMENTAL SECTION

The experimental setup, shown in Figure 1, has been described previously[17] with the exception of the frequency comb integration, so it will be discussed only briefly here. A Ytterbium-doped fiber laser is frequency modulated with a fiber-coupled electro optic modulator (EOM) using two RF generators: one at ∼80 MHz for heterodyne detection, and the other at ∼2 MHz for locking to the optical cavity around the discharge cell. After the modulation is applied, this seed laser is amplified to 10 W total power using a fiber amplifier, and this amplified beam acts as the pump for the optical parametric oscillator (OPO).

Three beams exit the OPO head: the pump (∼1064 nm), the signal (tunable from 1.5 to 1.6 μm), and the idler (tunable from 3.2 to 3.9 μm). The idler is used for spectroscopy of HCO^+, while the other beams are used for frequency measurements using a near-infrared wavemeter and frequency comb. For the comb-calibrated scans, the wavemeter is only used prior to a scan to determine which comb modes the pump and signal are each closest to, while the comb is used throughout the scan to take frequency readings at each acquired data point.

Comb Integration. The optical frequency comb used in this work (Menlo FC1500) has been described previously in operation with a different laser system.[18] In this work, the comb is used for both stabilizing and measuring the pump frequency. It is also used for measuring the frequency of the signal after it is shifted by a double-pass AOM. The shifted-signal frequency and the AOM frequency are then used to calculate the unshifted signal frequency, which when combined with the pump frequency measurement, are used to determine the frequency of the idler. A detailed explanation of the comb operation follows.

Scanning the OPO with the comb is accomplished by first tuning the carrier-envelope offset of the comb to approximately 20 MHz and determining its sign. Then the comb repetition rate is tuned to make the signal offset beat lie within the range of 25−35 MHz from the nearest comb mode, limited by the RF bandpass filter built into the frequency counter used to record that beat. Then the frequency of the pump is tuned to approximately 20 MHz from its nearest comb mode, and the signs of the offset beats for both the pump and the signal are determined and recorded. Finally, the pump is offset-locked to the comb using a frequency-to-voltage converter circuit that generates an appropriate error signal for offset locking.

The nearest comb mode numbers are determined for the pump and the signal before each scan using the wavemeter, then are recorded (and incremented/decremented for the signal when necessary) as the scan progresses. At each frequency step, the data acquisition program pauses for 1.5 s, then the comb repetition rate and offset beats are recorded by frequency counters with 1 Hz refresh rates, and the lock-in amplifier outputs are recorded. With the lock-in amplifier time constant set to 300 ms, the lock-in amplifiers have 5 time constants to respond before the reading is polled for each point, so any scanning direction dependent line center pulling is smaller than the random scan-to-scan variability in line center determination.

After each point, the repetition rate is tuned by an amount sufficient to slew the pump frequency by ∼5 MHz (∼1.8 Hz change in repetition rate). The pump remains offset locked to the same comb mode throughout the course of each scan. The total continuous scanning range of the pump (and therefore for the idler) for comb-calibrated scans is limited to ∼800 MHz by the comb scanning electronics; the comb repetition rate can only be changed by a relatively small amount while still retaining its lock onto the direct digital synthesizer (DDS) that stabilizes the repetition rate.

To keep the signal offset within the frequency counter bandpass filter at each point, a feed-forward system is used to tune the signal frequency using a double-pass acousto-optic modulator (AOM) setup. In a double-pass configuration, the frequency shift induced by the AOM is doubled, while making the pointing of the beam independent of the frequency applied

dx.doi.org/10.1021/jp400570m | J. Phys. Chem. A 2013, 117, 10034−10040

to the AOM.[19] Stable pointing is crucial to the operation of the system, as good spatial overlap between the comb light and each of the cw beams is important for generating offset beat signals on the high speed detectors.

After the counters are read for a data point and the repetition rate is slewed to the next point, the amount the signal frequency needs to be shifted by is calculated using the change in the repetition rate, the signal comb mode number, and the amount the signal was away from the 30 MHz target offset frequency for the previous point; this frequency shift is then applied to the frequency of the RF generator that drives the AOM. The AOM diffraction efficiency is high enough to provide reliable signal/comb offset beat measurements in the driving frequency range of 150−210 MHz, which corresponds to a frequency shift of 300−420 MHz when taking into account the double-pass configuration. When the calculated desired AOM frequency lies outside this range, the drive frequency is shifted by 50 MHz (corresponding to a 100 MHz change in the shifted signal frequency, matching the comb repetition rate), and the signal mode number is incremented or decremented by one, depending on whether the 100 MHz shift was positive or negative.

This signal-shifting scheme allows the shifted signal frequency to be determined using the frequency comb at each point, despite the fact that the signal frequency is fixed (with the exception of some slow drift) while the comb repetition rate is slewing. The unshifted signal frequency can then be determined simply by subtracting the AOM frequency shift, which is precisely known from the digital setting of the RF generator at each point, and this unshifted signal frequency is subtracted from the directly measured pump frequency to determine the idler frequency.

Spectroscopic Configuration. The plasma cell used in this work, Black Widow, shown in Figure 2, was the same cell

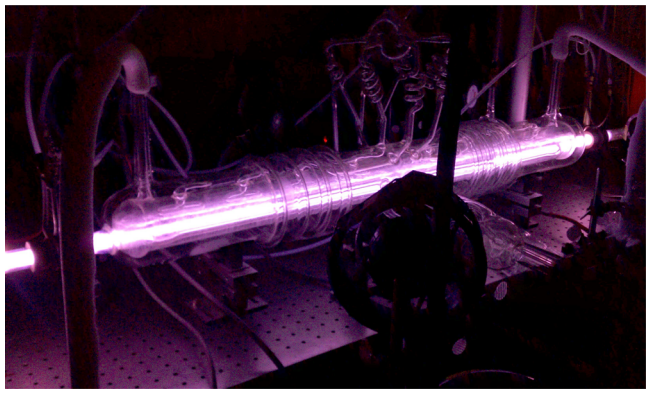

Figure 2. Black Widow, the liquid nitrogen cooled positive column discharge cell acquired from Takeshi Oka and used for the work in this article. The central bore, where the plasma discharge occurs, is surrounded by a sheath of flowing liquid nitrogen, which is in turn surrounded by a vacuum jacket to prevent ice from forming on the cell.

used by Takeshi Oka in many of his velocity modulation experiments. It allows for liquid nitrogen cooling of the plasma to reach an estimated rotational temperature of ∼166 K for HCO^+, as shown in the Boltzmann plot in Figure 3, using plasma conditions of 30 mTorr CO in 500 mTorr H_2 with a 35 kHz, 140 mA discharge. The idler beam is coupled through Brewster windows on either end of the cell into the central bore

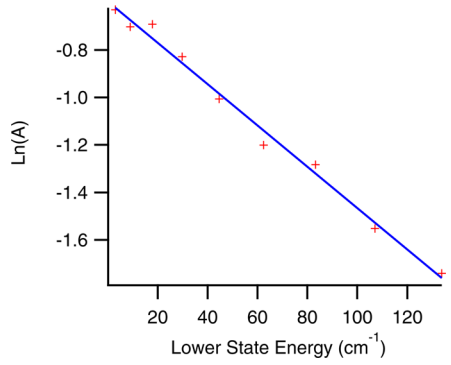

Figure 3. Boltzmann plot for R(1) through R(9), with the slope indicating a rotational temperature of ∼166 K. The vertical axis is the natural log of the line strength normalized peak-to-peak amplitude of a double-pass scan for each transition.

of the discharge cell. For this work, three different optical configurations were used: single-pass, double-pass, and cavity-enhanced, all of which relied on heterodyne modulation and detection at ∼80 MHz.

The comb calibrated scans presented in this article used a simple single-pass configuration, as shown in Figure 1. This allowed for the acquisition of Doppler-broadened scans with signal-to-noise ratios of ∼300 for the strongest lines and ∼100 for the weakest ones but, because of the lack of a bidirectional beam and sufficient laser power, did not allow for the observation of Lamb dips. A typical comb-calibrated scan is shown in Figure 4.

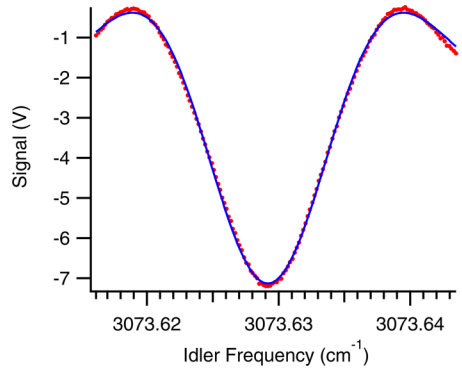

Figure 4. Typical comb-calibrated scan (red dots) of the P(5) transition of HCO^+, along with a fit to the data (blue line). Error bars for the points are not shown, as they would be smaller than the point size for both intensity and frequency.

A series of double-pass wavemeter-calibrated scans were collected for the previously unobserved P(11) through P(17) transitions. In the double-pass configuration, a single mirror was placed on the far side of the cell to back-reflect the idler for a second pass through the cell. Approximately 30% of the reflected beam was then picked off with a silicon window and directed to a high-speed detector, the signal from which was demodulated first at the heterodyne frequency, then at twice the plasma frequency ($2f$), as opposed to the $1f$ demodulation that was used for the single-pass work.

A few uncalibrated scans were collected with the laser frequency locked to an optical cavity positioned around the discharge cell, in a noise immune cavity enhanced optical heterodyne velocity modulation spectroscopy (NICE−

dx.doi.org/10.1021/jp400570m | J. Phys. Chem. A 2013, 117, 10034−10040

OHVMS)[20] configuration, as was done by Crabtree et al.[17] One such scan, showing strong central Lamb dip features on top of the Doppler profile, is shown in Figure 5. In this experiment,

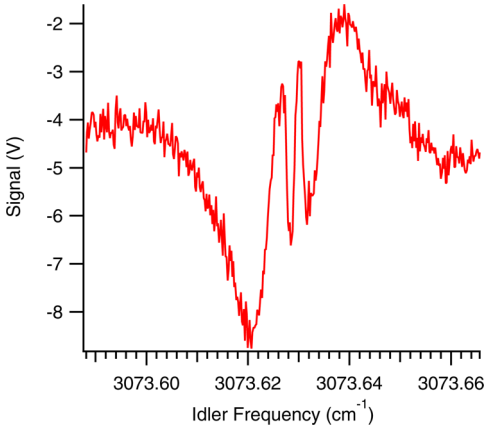

Figure 5. Roughly calibrated scan of the P(5) transition of HCO^+, showing the Lamb dips that are obtainable with cavity enhancement combined with lower cell pressure. The frequency calibration of this scan was based on the line center determined from the comb calibrated scans combined with the approximate scan voltage to frequency transfer function of the seed laser.

cavity enhancement is combined with 2*f* demodulation, making detection sensitive to not only velocity modulation but also concentration modulation of the ions of interest. This detection scheme allows for the observation of Lamb dips as the zero-velocity population of ions is modulated throughout the course of a discharge cycle.

Unfortunately, the dielectric coatings on the mirrors were found to be hygroscopic, which led to poor laser coupling efficiency through the cavity in this wavelength range and degraded performance over time. To obtain optimal Lamb dip depth, the total cell pressure had to be decreased to ∼200 mTorr, and the discharge current had to be turned down as low as possible while still maintaining a stable plasma, to ∼100 mA. Both the lower pressure and the lower discharge current produce lower overall density of HCO^+ within the cell. This decreased density combined with the poor laser transmission through the cavity cause the signal-to-noise in the NICE−OHVMS scans to be significantly compromised compared to the single- and double-pass scans, despite the factor of ∼400 greater path length that NICE−OHVMS provides through the plasma.

RESULTS AND DISCUSSION

Each comb calibrated scan was fit to a second derivative of a Gaussian function, which approximates the convolution of heterodyne modulation with velocity modulation observed in the experiment. As can be seen in Figure 4, the fit is not perfect, especially near the outer lobes of the line shape. Lineshapes in velocity modulation experiments are often significantly more complex than simple derivatives of ordinary unmodulated lineshapes,[5] but for the purposes of determining line centers, the chosen function is sufficient. Between 4 and 7 scans were acquired of each transition, and the data acquired from those fits were used to compute the average line centers and standard errors shown in Table 1. The errors varied somewhat from one transition to the next, but the average uncertainty was found to be ∼600 kHz.

Table 1. List of the Comb-Calibrated HCO^+ Transition Center Frequencies (With Associated Uncertainties) Observed in the Current Work, Compared with Previous Measurements

transition	line center (cm^{-1})	previous work[6] (cm^{-1})	previous − current (MHz)
R(0)	3091.690432(16)	3091.6919(10)	44
R(1)	3094.618099(27)	3094.6181(10)	0
R(2)	3097.522054(07)	3097.5223(10)	7
R(3)	3100.402249(25)	3100.4034(10)	35
R(4)	3103.258604(21)	3103.2586(10)	0
R(5)	3106.090956(19)	3106.0909(10)	−2
R(6)	3108.899376(20)	3108.9002(10)	25
R(7)	3111.683680(04)	3111.6841(10)	13
R(8)	3114.443835(05)	3114.4445(10)	20
R(9)	3117.179881(41)	3117.1800(10)	4
P(1)	3085.763903(23)	3085.7646(10)	21
P(2)	3082.765487(53)	3082.7662(10)	21
P(3)	3079.743422(15)	3079.7437(10)	8
P(4)	3076.698005(05)	3076.6977(10)	−9
P(5)	3073.629188(16)	3073.6291(10)	−3
P(6)	3070.537136(19)	3070.5377(10)	17
P(7)	3067.421924(37)	3067.4224(10)	14
P(8)	3064.283464(10)	3064.2834(10)	−2
P(9)	3061.122045(18)	3061.1226(10)	17
P(10)	3057.937606(08)	3057.9380(10)	12

As can be seen by the fit in Figure 4, this fit function is not perfect, likely due to imperfect setting of the detection phases. For this work, both the RF and plasma demodulation phases were set to maximize the signal-to-noise of a single detection channel out of the four channels that were acquired with each scan. It is likely that there is some dispersive component to the line shape function, rather than it being purely absorptive. It is also likely that the velocity modulation of the ions is not purely sinusoidal and that the lock-in demodulation is not exactly in phase with the velocity modulation, and both of these factors can also affect the overall line shape.

There is also a slight asymmetry in the observed line shapes for several of the scans that is not fully understood at this time. By adding a slightly sloped baseline to the data, we can make it significantly more symmetric and also make the fit slightly better. Symmetrizing the data in this way causes the determined line center to shift by less than 1 MHz for even the most asymmetric scans. Given that we do not know the physical cause of this phenomenon, we have taken the approach of manipulating the data as little as possible, so this symmetrizing was only done to estimate the potential error induced by the asymmetry.

When asymmetry is present, it tends to manifest with the low-frequency lobe of the line shape having a greater maximum than the high-frequency one, although by tuning detection phases and plasma conditions, we are able to reverse the asymmetry, making the high-frequency lobe larger. Fitting the same line with opposite asymmetry slopes provides line centers that are shifted by less than 1 MHz relative to one another, providing further evidence that any asymmetry-induced errors in line center determination must be fairly small, on the order of 1 MHz or smaller.

All of the comb-calibrated data presented in this work was performed with the identical phase settings and plasma conditions, leading to line shapes that were similarly

dx.doi.org/10.1021/jp400570m | J. Phys. Chem. A 2013, 117, 10034−10040

asymmetric. Such a systematic error would be mitigated by subtraction of observed line centers, as is done in the combination differences analysis described in the following several paragraphs. On the basis of the errors in the calculation of rotational transitions, it appears that random scan-to-scan variability is the limiting factor in line center determination and not the effects of this asymmetry.

For approximately half of the comb-calibrated scans, the determined line centers disagreed with the previously measured HCO^+ transition frequencies[6] by greater than the specified accuracy of 30 MHz. It was found that the source of the errors was incorrect comb mode number determination for either the signal or the pump beams due to inaccuracy of the wavemeter. These incorrectly calibrated scans were easily corrected by adding or subtracting a multiple of the comb repetition rate to or from the calculated idler frequency. After correcting the idler frequency calibration, it was found that all but two of the observed transitions agreed with Amano's previous work to within 30 MHz. The two exceptions to the 30 MHz agreement were the R(0) and R(3) transitions, but those were both further verified by comparing the combination difference analysis with directly measured rotation transitions, as shown in Table 2. Any remaining error in the determination of comb mode numbers would appear as an error of ∼100 MHz, which is not observed.

Table 2. Indirectly Calculated Rotational Transition Frequencies Derived from the Data in Table 1 Compared to the Directly Measured Rotational Transitions Compiled by Cazzoli et al.[15]

J'	J''	calc freq (MHz)	obs freq[15] (MHz)	calc − obs (MHz)
0	1	n/a	89188.5247	n/a
1	2	178374.6(17)	178375.0563	−0.5
2	3	267557.0(19)	n/a	n/a
3	4	356732.3(19)	356734.2230	−2.0
4	5	445903.9(21)	445902.8721	1.0
5	6	535061.0(23)	535061.5810	−0.5
6	7	624207.4(26)	624208.3606	−1.0
7	8	713344.0(27)	713341.2278	2.8
8	9	802455.7(27)	802458.1995	−2.5
9	10	891558.4(27)	891557.2903	1.1

A combination differences analysis was performed to demonstrate the accuracy of our comb-calibrated rovibrational compared to known rotational transitions. First, frequencies of transitions sharing the same upper state energy level, e.g., R(0) and P(2), were subtracted from one another to generate ground state energy level spacings for pairs of energy levels separated by two rotational energy levels. For example, the $J = 2 \leftarrow 0$ spacing was calculated from $f_{R(0)} - f_{P(2)}$, the $J = 3 \leftarrow 1$ spacing was calculated from $f_{R(1)} - f_{P(3)}$, and so forth for all observed transitions up to the $J = 10 \leftarrow 8$ spacing.

Then the directly measured $J = 1 \leftarrow 0$ transition was subtracted from the $J = 2 \leftarrow 0$ energy level spacing to indirectly compute the $J = 2 \leftarrow 1$ rotational transition frequency. This computed frequency was then subtracted from the $J = 3 \leftarrow 1$ spacing to compute the $J = 3 \leftarrow 2$ transition frequency, and the process was repeated for higher rotational energy levels up to $J = 10 \leftarrow 9$. At each step, the calculated rotational transition from the previous step was used with a new energy level difference to compute a new rotational transition. The indirectly calculated rotational transitions in the current work are compared to the previously observed rotational transition frequencies in Table 2.

Such an analysis was also carried out for the ν_1 (C−H stretch mode) first vibrationally excited state. To our knowledge, the only directly observed rotational transition was $J = 3 \leftarrow 2$.[16] This single transition, combined with our rovibrational data, is sufficient to compute the expected rotational transitions from $J = 1 \leftarrow 0$ up to $J = 10 \leftarrow 9$, as shown in Table 5.

The rovibrational comb-calibrated data were also fit to a simple Hamiltonian to determine the constants shown in Table 3, where the quartic distortion terms for the lower and upper vibrational states were constrained to be equal to one another. The full results of the fit, showing the deviations of the data from the fit result, is shown in Table 4. The experimental data agree with the fit within 2σ for all but three of the observed transitions, and all of the data agree with the fit to within 4σ. This provides further evidence for the internal consistency of this rovibrational data set, and validation that the random errors that contribute to the statistical uncertainties are the limiting factor of the accuracy and precision (as oppposed to other effects that vary from one line to the next, such as the observed asymmetry in the lineshapes).

Table 3. Molecular Constants (And Associated Uncertainties) Obtained from a Least Squares Fit of the Full Comb-Calibrated Rovibrational Data Set; Full Fit Results, Including the Associated Residuals, Are Given in Table 4

constant	value (MHz)
ν_0	92598065.20(19)
B''	44594.166(25)
B'	44240.297(27)
D''	−0.07784(49)
D'	−0.07760(49)
$H' = H''$	$-0.0269(28) \times 10^{-3}$

Table 4. Full Results of the Least Squares Fit of the Full Comb-Calibrated Rovibrational Data Set

J'	J''	obs freq (cm^{-1})	calc freq (cm^{-1})	obs − calc (cm^{-1})
0	1	3091.690432(16)	3091.690368	0.000064
1	2	3094.618099(27)	3094.618083	0.000016
2	3	3097.522054(07)	3097.522065	−0.000011
3	4	3100.402249(25)	3100.402251	−0.000002
4	5	3103.258604(21)	3103.258575	0.000030
5	6	3106.090956(19)	3106.090968	−0.000012
6	7	3108.899376(20)	3108.899361	0.000015
7	8	3111.683680(04)	3111.683678	0.000002
8	9	3114.443835(05)	3114.443840	−0.000005
9	10	3117.179881(41)	3117.179764	0.000117
1	0	3085.763903(23)	3085.763992	−0.000089
2	1	3082.765487(53)	3082.765454	0.000033
3	2	3079.743422(15)	3079.743436	−0.000014
4	3	3076.698005(05)	3076.698000	0.000005
5	4	3073.629188(16)	3073.629214	−0.000026
6	5	3070.537136(19)	3070.537148	−0.000012
7	6	3067.421924(37)	3067.421874	0.000050
8	7	3064.283464(10)	3064.283471	−0.000007
9	8	3061.122045(18)	3061.122020	0.000025
10	9	3057.937606(08)	3057.937608	−0.000002

In addition to the comb-calibrated scans that were collected for the combination differences analysis, several previously unobserved P-branch transitions were recorded with only

dx.doi.org/10.1021/jp400570m | J. Phys. Chem. A 2013, 117, 10034−10040

wavemeter calibration. All but one of the linecenters determined from these scans fall within the expected 70 MHz uncertainty from the wavemeter calibration. The one exception, P(17), is thought to be off by more than the uncertainty due to an inaccurate signal wavelength reading caused by poor optical alignment of the wavemeter. These transitions, whose frequencies are given in Table 6, could not be used for combination differences calculations because their corresponding R-branch transitions lie outside the tuning range of our current OPO module, though additional tuning could be obtained with other modules.

Table 5. Pure Rotational Transitions for the Vibrationally Excited ν_1 State of HCO^+, Calculated from the Rovibrational Data in Table 1 and the Directly Observed[21] $J = 3 \leftarrow 2$ Rotational Transition

J'	J''	calc freq (MHz)	uncertainty (MHz)
0	1	88486.7	1.9
1	2	176955.4	1.6
2	3	n/a	n/a
3	4	353900.7	0.9
4	5	442366.0	1.1
5	6	530813.3	1.3
6	7	619257.7	1.6
7	8	707676.3	1.9
8	9	796093.7	1.9
9	10	884477.9	2.4

Table 6. Previously Unobserved Wavemeter-Calibrated Scans of the P(11) through P(17) Transitions[a]

transition	obs (cm^{-1})	calc (cm^{-1})	obs − calc (MHz)
P(11)	3054.730	3054.73019(4)	−6
P(12)	3051.502	3051.49993(5)	62
P(13)	3048.245	3048.24688(6)	−57
P(14)	3044.969	3044.97111(7)	−63
P(15)	3041.672	3041.67269(8)	−21
P(16)	3038.354	3038.35169(9)	69
P(17)	3035.013	3035.00817(10)	145

[a]Uncertainties are ∼70 MHz, limited by the wavemeter uncertainties for the pump and signal frequencies added in quadrature. Calculations are based on ground state constants from Cazzoli et al.,[15] and excited state constants are determined from our comb-calibrated scans.

CONCLUSIONS

The current work demonstrates the ability of Doppler-broadened comb-calibrated velocity modulation spectroscopy to determine line centers with sub-MHz accuracy and precision. This accuracy has been verified by performing a combination differences analysis of the rovibrational data and comparing the results to the previously observed rotational spectrum of vibrational ground state HCO^+. The potential of extending the technique to sub-Doppler work has also been demonstrated. With a proper set of cavity mirrors, it should be possible to further improve the precision of this technique. From the current series of fits, the Doppler-limited line width is ∼450 MHz, and the uncertainty of a single fit is ∼350 kHz. From the Lamb dip scan of HCO^+ shown in Figure 5, the peak-to-peak line width of the central sub-Doppler feature is only ∼50 MHz, so it is reasonable to assume that the precision of a fit to sub-Doppler features would be approximately an order of magnitude more precise than one to a Doppler-broadened scan, assuming the S/N problem can be solved by a non-hygroscopic set of cavity mirrors. The investigation into whether the accuracy is also improved by the same factor will be the subject of future work.

One of the greatest advantages of this indirect approach over direct rotational spectroscopy is the generality of it. The chemistry within positive column discharge cells tends to be very rich, so it is possible to make a wide variety of molecular ions. The cell used in the current work was cooled with liquid nitrogen, but it could easily be cooled by water or air, or even heated to attain greater population in higher rotational levels and compute the rotational spectrum up to very high J values. The infrared source and detectors are also very versatile in terms of spectral coverage; entire rovibrational bands for a wide variety of ions lie within its tuning range and can be observed without any changes to the optoelectronic system.

This work also has implications for astronomical searches for the astrophysically relevant ion HCO^+. While the ground vibrational state has been thoroughly studied, little work has previously been done in this vibrationally excited state. Rotational transitions in the vibrationally excited state could be of astrophysical interest, particularly in hot, dense environments such as hot cores and circumstellar envelopes.[22]

AUTHOR INFORMATION

Corresponding Author

*(B.J.M.) E-mail: bjmccall@illinois.edu.

Notes

The authors declare no competing financial interest.

ACKNOWLEDGMENTS

We would like to acknowledge an NSF grant (CHE 12-13811) and a NASA Laboratory Astrophysics grant (NNX13AE62G) for funding. B.J.M. wishes to acknowledge support from a David & Lucile Packard Fellowship and a Camille Dreyfus Teacher-Scholar award. B.M.S. would like to thank a NASA Earth and Space Science Fellowship (NESSF NNX11AO06H), and J.N.H. is grateful for support by a Robert & Carolyn Springborn fellowship and an NSF Graduate Research Fellowship (DGE 11-44245 FLLW). We would also like to thank Takeshi Oka for supplying the discharge cell and associated electronics and pumps used for this work.

REFERENCES

(1) Wing, W.; Ruff, G.; Lamb, W.; Spezeski, J. Observation of the Infrared Spectrum of the Hydrogen Molecular Ion HD^+. *Phys. Rev. Lett.* **1976**, *36*, 1488−1491.

(2) Gudeman, C. S.; Begemann, M. H.; Pfaff, J.; Saykally, R. J. Velocity-Modulated Infrared Laser Spectroscopy of Molecular Ions: The ν_1 Band of HCO^+. *Phys. Rev. Lett.* **1983**, *50*, 727−731.

(3) Stephenson, S. K.; Saykally, R. J. Terahertz Laser Velocity Modulation Spectroscopy of Ions. *J. Mol. Spectrosc.* **2005**, *231*, 145−153.

(4) Gudeman, C. S.; Saykally, R. J. Velocity Modulation Infrared Laser Spectroscopy of Molecular Ions. *Annu. Rev. Phys. Chem.* **1984**, *35*, 387−418.

(5) Farley, J. Theory of the Resonance Line-Shape in Velocity-Modulation Spectroscopy. *J. Chem. Phys.* **1991**, *95*, 5590−5602.

(6) Amano, T. The ν_1 Fundamental Band of HCO^+ by Difference Frequency Laser Spectroscopy. *J. Chem. Phys.* **1983**, *79*, 3595.

(7) Verbraak, H.; Ngai, A. K. Y.; Persijn, S. T.; Harren, F. J. M.; Linnartz, H. Mid-Infrared Continuous Wave Cavity Ring Down

Spectroscopy of Molecular Ions Using an Optical Parametric Oscillator. *Chem. Phys. Lett.* **2007**, *442*, 145−149.
(8) Buhl, D.; Snyder, L. E. Unidentified Interstellar Microwave Line. *Nature* **1970**, *228*, 267−269.
(9) Klemperer, W. Carrier of the Interstellar 89.190 GHz Line. *Nature* **1970**, *227*, 1230−1230.
(10) Woods, R.; Dixon, T.; Saykally, R.; Szanto, P. Laboratory Microwave Spectrum of HCO^+. *Phys. Rev. Lett.* **1975**, *35*, 1269−1272.
(11) Sanchez Contreras, C.; Sahai, R. Physical Structure of the Protoplanetary Nebula CRL 618. II. Interferometric Mapping of Millimeter-Wavelength HCN J = 1−0, HCO^+ J = 1−0, and Continuum Emission. *Astrophys. J.* **2004**, *602*, 960−977.
(12) Purcell, C. R.; Balasubramanyam, R.; Burton, M. G.; Walsh, A. J.; Minier, V.; Hunt-Cunningham, M. R.; Kedziora-Chudczer, L. L.; Longmore, S. N.; Hill, T.; Bains, I.; et al. A CH_3CN and HCO^+ Survey Towards Southern Methanol Masers Associated with Star Formation. *Mon. Not. R. Astron. Soc.* **2006**, *367*, 553−576.
(13) Liszt, H.; Lucas, R. mm-wave HCO^+, HCN and CO Absorption Toward NGC-1052. *Astron. Astrophys.* **2004**, *428*, 445−450.
(14) Milam, S. N.; Savage, C.; Ziurys, L. M.; Wyckoff, S. HCO^+ Observations Toward Comet Hale-Bopp (C/1995 O1): Ion−Molecule Chemistry and Evidence for a Volatile Secondary Source. *Astrophys. J.* **2004**, *615*, 1054−1062.
(15) Cazzoli, G.; Cludi, L.; Buffa, G.; Puzzarini, C. Precise THz Measurements of HCO^+, N_2H^+, and CF^+ for Astronomical Observations. *Astrophys. J., Suppl. Ser.* **2012**, *203*, 11.
(16) Lattanzi, V.; Walters, A.; Drouin, B. J.; Pearson, J. C. Rotational Spectrum of the Formyl Cation, HCO^+, to 1.2 THz. *Astrophys. J.* **2007**, *662*, 771−778.
(17) Crabtree, K. N.; Hodges, J. N.; Siller, B. M.; Perry, A. J.; Kelly, J. E.; Jenkins, P. A., II; McCall, B. J. Sub-Doppler Mid-Infrared Spectroscopy of Molecular Ions. *Chem. Phys. Lett.* **2012**, *551*, 1−6.
(18) Mills, A. A.; Siller, B. M.; McCall, B. J. Precision Cavity Enhanced Velocity Modulation Spectroscopy. *Chem. Phys. Lett.* **2010**, *501*, 1−5.
(19) Donley, E. A.; Heavner, T. P.; Levi, F.; Tataw, M. O.; Jefferts, S. R. Double-Pass Acousto-Optic Modulator System. *Rev. Sci. Instrum.* **2005**, *76*, 063112.
(20) Siller, B. M.; Porambo, M. W.; Mills, A. A.; McCall, B. J. Noise Immune Cavity Enhanced Optical Heterodyne Velocity Modulation Spectroscopy. *Opt. Express* **2011**, *19*, 24822−24827.
(21) Hirota, E.; Endo, Y. Microwave Spectroscopy of HCO^+ and DCO^+ in Excited Vibrational States. *J. Mol. Spectrosc.* **1988**, *127*, 527−534.
(22) Blake, G. A.; Laughlin, K. B.; Cohen, R. C.; Busarow, K. L.; Saykally, R. J. Laboratory Measurement of the Pure Rotational Spectrum of Vibrationally Excited HCO^+ (ν_2 = 1) by Far-Infrared Laser Sideband Spectroscopy. *Astrophys. J.* **1987**, *316*, L45−L48.

■ NOTE ADDED AFTER ASAP PUBLICATION

This article was published ASAP on July 3, 2013. After this paper was finalized, comb-calibrated sub-Doppler spectra were obtained for the P(5) and R(3) transitions, and the line centers were 4.1(6) and 3.7(8) MHz, respectively, lower than the values in Table 1 from our single-pass measurements. This evidently systematic offset is likely due to an asymmetry in the ion drift velocity in our AC plasma, and does not affect the indirect rotational transitions reported here as the offset is removed by subtraction. Since the observed Lamb dips probe only the zero-velocity ion population, we expect their frequencies to be independent of any plasma asymmetry. The corrected version was published ASAP on July 10, 2013.